Int. J. Heat Mass Transfer. Vol. 28, No. 12, pp. 2247–2259, 1985
Printed in Great Britain

0017–9310/85 $3.00 + 0.00

Heat transfer and pressure drop results for one- and two-row arrays of finned tubes

E. M. SPARROW and F. SAMIE*
Department of Mechanical Engineering, University of Minnesota, Minneapolis, MN 55455, U.S.A.

(*Received* 2 *March* 1985 *and in final form* 11 *June* 1985)

Abstract—Experiments were performed to measure Nusselt numbers and pressure loss coefficients for annular-finned tubes deployed in either a one-row array or in an in-line or a staggered two-row array. The apparatus was electrically heated and air was the convective heat transfer medium. The transverse and longitudinal pitches were varied parametrically and, for each configuration, the freestream Reynolds number ranged from 7500 to 32,000. For the one-row arrays, both the Nusselt number and the pressure loss coefficient were highly sensitive to the transverse pitch. The Nusselt numbers for the first row of a two-row array did not deviate appreciably from those of the corresponding one-row array, with the greatest deviations occurring for staggered arrays having intermediate values of the longitudinal pitch. For the tubes of the second row, the Nusselt numbers for the staggered arrays generally exceeded those for the in-line arrays and were also less sensitive to the longitudinal pitch. The overall pressure drops for the two-row, staggered arrays were also quite insensitive to the pitch, with values that were about twice those for the corresponding one-row array. On the other hand, the pressure drops for the in-line arrays were always less than twice the one-row values, with a tendency to increase with increasing longitudinal pitch.

INTRODUCTION

BANKS of finned tubes are employed in a very broad range of heat exchanger applications. Notwithstanding this, there are significant gaps in the archival literature with regard to heat transfer and pressure drop data for finned tubes. In particular, there are virtually no data for in-line arrays. For staggered configurations, all of the reported heat transfer and pressure drop information was obtained from experiments on arrays made up of a large number of rows (e.g., eight or more rows for the heat transfer experiments). More to the point, no prior work appears to have been performed for one- and two-row finned tube banks, which are the subject of the experimental study that is reported here.

The present experimental program was subdivided into three parts in accordance with the configuration of the investigated arrays. The first part dealt with the one-row array, for which the dimensionless transverse pitch was varied parametrically in six steps. Both the second and third parts were concerned with two-row arrays, respectively for in-line and staggered configurations. For both the in-line and staggered arrays, the longitudinal pitch was varied over a six-step range while the transverse pitch was held fixed at a value relevant to practice.

Measurements were made to determine both the heat transfer and pressure drop characteristics. For the two-row array, heat transfer coefficients were measured separately in the first and second rows. For each of the 18 array configurations for which experiments were performed, the Reynolds number (based on the freestream velocity and the diameter of the base tube) was varied parametrically from 7500 to 32,000. The experiments were performed in air in a low-turbulence wind tunnel.

The finned tubes used in the experiments were equipped with annular fins. In order to avoid thermal contact resistance, the fins were made integral with the base tube. Furthermore, the experiments were designed to circumvent the uncertainties inherent in the determination of external airside heat transfer coefficients from overall measurements in a two-fluid heat exchanger (i.e. the conventional method). To this end, only a single fluid (air) was used and the role of the second fluid was fulfilled by electrical heating. In addition, to attain well-defined thermal boundary conditions, guard heating was used, and the thermal conductivity and thicknesses of the fins and the tube wall were chosen so that the base tube was virtually isothermal and the fin efficiency near unity.

The available relevant literature is limited to experiments on staggered, many-rowed, two-fluid heat exchangers [1–5]. The finned tubes investigated in [1–3] were helically finned, while those of [4] were equipped with elliptical studs. In [5], a variety of commercially available fin types were tested. An annular-finned heat exchanger model employed in [6] consisted of a single tube in each row, with two half tubes positioned adjacent to the sidewalls of the flow passage in alternate rows. Heat transfer correlations for staggered, many-rowed arrays of finned tubes are presented in [3] and [7], while pressure drop correlations are given in [1–3] and [8].

EXPERIMENTAL APPARATUS

The description of the experimental apparatus is facilitated by reference to Figs. 1 and 2. The first of these

* Present address: General Motors Research Laboratories, Warren, Michigan, U.S.A.

NOMENCLATURE

A_b exposed area of base tube
A_f fin surface area (annular faces and tips)
D diameter of base tube
D_f diameter of fin tips
h per-tube heat transfer coefficient, equation (4)
K_{pm} pressure loss coefficient, $\Delta p/\frac{1}{2}\rho U_m^2$
$K_{p\infty}$ pressure loss coefficient, $\Delta p/\frac{1}{2}\rho U_\infty^2$
k thermal conductivity
L tube length
Nu per-tube Nusselt number, hD/k
Δp array pressure drop
Q rate of heat transfer
Re_m minimum-area Reynolds number, $\rho U_m D/\mu$
Re_∞ freestream Reynolds number, $\rho U_\infty D/\mu$
S_L longitudinal pitch between tube centers
S_T transverse pitch between tube centers
s spacing between fins on a given tube
T_b base tube temperature
T_∞ freestream temperature
t fin thickness
U_m superficial velocity in minimum free flow area
U_∞ freestream velocity upstream of array.

Greek symbols
β angular coordinate around circumference
Δ transverse distance between fin tips of adjacent tubes
η fin efficiency
μ viscosity
ρ density.

Other symbols
$\bar{}$ circumferential average.

is a side view showing one of the finned tubes in place in the wind tunnel in which the experiments were performed. As depicted there, the tubes were mounted with their axes vertical and occupied the entire height of the wind tunnel. The tunnel cross section was a 30.48 × 60.96 cm (1 × 2 ft) rectangle, height × width, with a 2.44 m (8 ft) streamwise length. The finned tube arrays were positioned well away from the inlet and exit cross sections. During the course of the experiments, the tunnel was operated in the range of freestream velocities from about 4 to 16 m s^{-1} (13 to 53 ft s^{-1}), with a freestream turbulence level of 0.4–0.5%.

The layout of the finned tubes is illustrated in Fig. 2. The figure is a top view looking down on representative arrays of tubes. Attention may first be focused on the first row of Fig. 2(a), with the remainder of the figure being regarded as absent. That row depicts the layout of the one-row array with seven tubes in place. One-row arrays consisting of 3, 5, 8, 9 and 10 tubes were also investigated. Note that in the positioning of the sidewall-adjacent tubes, the distance between the fin tips and the wall was set at $\Delta/2$, where Δ is the transverse distance between the fin tips of adjacent tubes in the array.

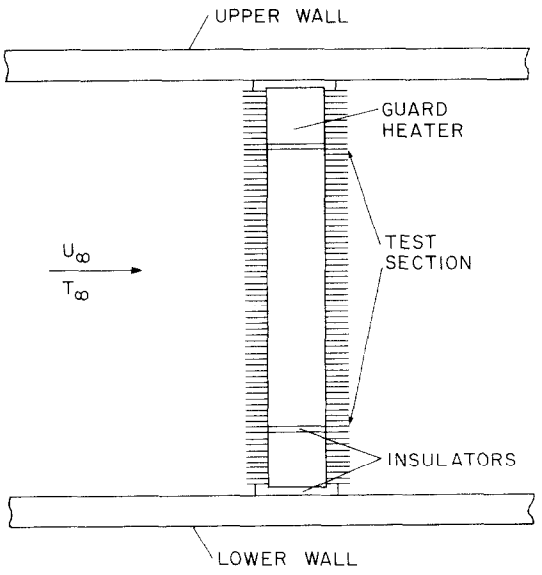

FIG. 1. Heated finned tube in place in the wind tunnel.

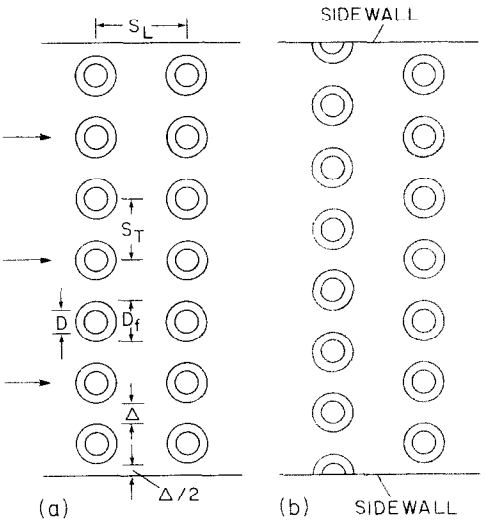

FIG. 2. Layout of the finned tubes.

In addition to Δ, the other dimensional nomenclature relevant to the one-row array includes the diameter D of the base tube, the diameter D_f of the fin tips, and the transverse pitch S_T between the tube centers. Both D and D_f were held fixed during the course of the experiments. For the one-row array, the transverse pitch was varied in accordance with the number of tubes in the array. For arrays with 10, 9, 8, 7, 5 and 3 tubes, the corresponding values of the dimensionless transverse pitch are

$$S_T/D_f = 1.07, 1.19, 1.33, 1.52, 2.13 \text{ and } 3.56. \quad (1)$$

The two-row, in-line array is illustrated by the two rows depicted in Fig. 2(a), with the same dimensional nomenclature as before and with the addition of S_L to denote the longitudinal pitch between tube centers. The transverse pitch S_T/D_f was held fixed at the practically-relevant value of 1.52, which corresponds to the layout shown in the figure. Parametric variations were made in the longitudinal pitch, yielding the dimensionless values

$$S_L/D_f = 1.26, 1.52, 1.79, 2.05, 3.10 \text{ and } 5.20. \quad (2)$$

The last two of these are well beyond the practical range and were included to explore the conditions under which the two-row array reverts to two independent one-row arrays.

Figure 2(b) illustrates the two-row staggered array. As seen in the figure, the staggering was achieved by the use of sidewall-adjacent half tubes in one of the rows. In common with the in-line array of Fig. 2(a), the transverse spacing for the staggered array was fixed at $S_T/D_f = 1.52$. Also in common were the investigated longitudinal pitches, i.e. those given by equation (2). The use of common values of S_T/D_f and S_L/D_f for the two types of arrays facilitates comparisons of their heat transfer and pressure drop characteristics.

In the execution of the heat transfer experiments, an approach commonly employed in laboratory investigations of crossflow tube banks was adopted, namely, that only one of the tubes in the array is heated while the others serve to establish the fluid flow. In the present experiments, the heated tube was positioned wherever heat transfer information was being sought—in the one-row array, in the first row of a two-row array and in the second row of a two-row array. In all cases, the heated tube was centered between the sidewalls to minimize effects associated with the transverse finiteness of the arrays.

The heated tube and the unheated tubes were of identical external dimensions as follows:

$$D_f/D = 1.8, s/D = 1/10, t/D = 1/30, L/D - 9.5 \quad (3)$$

where s is the spacing between the fins, t is the fin thickness, and L is the overall length of the tube. The base tube diameter D was 3.175 cm (1.25 in.). There are six fins per in., a value that is commonly encountered in practice. As noted earlier, the fins are annular.

Each of the unheated tubes was fabricated from a solid aluminum rod whose surface was circumferentially grooved to create the interfin spaces. The heated tube was a composite structure whose main features will now be discussed.

The heated tube is shown schematically in Fig. 1. As seen there, it consisted, in the main, of a central portion (the heated test section) flanked at either end by a guard heater. Both the test section and the guard heaters were fabricated from solid aluminum rod stock, into which integral annular fins were machined by circumferentially grooving the external surface of the rod.

The respective sections of rod were bored along their axes to provide the finned tube with a hollow center. The wall thickness of the circular cross section which resulted from the boring operation was 0.635 cm (0.250 in.)—a relatively thickwalled tube. Uniformly wound heater cores, specifically fabricated for the present apparatus, were installed in the test section and the guard sections. The heater cores were, themselves, hollow to enable the passage of power leads and thermocouple wires.

Eight pre-calibrated, fine-gage chromel–constantan thermocouples were installed in the test section, and each guard heater was equipped with three thermocouples. The thermocouple junctions were positioned to be about 0.076 cm (0.030 in.) from the surface of the base tube that was exposed to the airflow in the interfin spaces. The thermocouple leads from the junctions were led radially inward into the hollow bore of the heater core and then axially upward and out the end of the tube (a detailed description of the thermocouple installation is available in ref. [9]). By design, the test section and the guard heaters could be rotated as a unit about the axis of the finned tube, thereby enabling the thermocouples to be positioned at any circumferential location relative to the freestream direction. In the execution of the experiments, temperature measurements were made at 30° intervals around the circumference.

To facilitate the elimination of extraneous conduction losses from the test section, the test section heater and the respective guard heaters were made separately controllable. During each data run, the temperatures of the adjacent portions of the test section and the guard heaters were matched by balancing the readings of suitably positioned thermocouples. To increase the sensitivity of the temperature-matching procedure, insulating spacers made of Delrin plastic were positioned between the respective ends of the test section and the guard heaters. Insulating disks, also of Delrin, were situated at the upper and lower ends of the finned tube to minimize heat flow by conduction from the guard heaters to the walls of the wind tunnel. Power for the test section and guard heaters was provided by a regulated AC supply.

The temperature T_∞ of the freestream flow approaching the array was measured by three thermocouples situated about 12 cm upstream of the first row and positioned off-center so that their wakes would not disturb the heated tube. All thermocouple outputs were read to 1 μV.

An L-shaped impact probe, used in conjunction with a contiguous wall static tap to measure the freestream velocity U_∞, was installed 25 cm upstream of the array, also off-center. In exploratory runs, the probe was transversed perpendicular to the wind tunnel wall in order to establish its proper positioning (i.e. outside the boundary layer). The aforementioned upstream wall static tap was also used together with another wall tap situated about 60 cm downstream of the array in order to determine the pressure drop caused by the presence of the array. The pressure drop runs were made without heat transfer. All pressure differences were measured with a Baratron solid-state pressure meter with a resolution of 10^{-3} Torr.

In supplementary data runs, the impact probe was installed immediately upstream of the array in order to explore possible precursive disturbances of the flow field caused by the blockage created by the array. In this installation, the tip of the probe was situated about 2.5 cm upstream of the forward edge of the array. The probe was traversed in the spanwise direction, so that it sensed the flow ahead of both the tubes and the intertube spaces. Traverses were also made in the direction of the tube axes (i.e. in the vertical direction).

DATA REDUCTION

The average heat transfer coefficients for the heated tube were determined by introducing the experimental data into the defining equation

$$h = Q/\overline{(T_b - T_\infty)}(A_b + \eta A_f) \tag{4}$$

where all quantities pertain to the test section portion of the tube. The rate of heat transfer Q was obtained directly from the electric power input to the test section heater. Corrections were not necessary since conduction losses were eliminated by the guard heating and radiation losses were estimated to be negligible by calculation. The quantity $\overline{(T_b - T_\infty)}$ is the circumferential average of the difference between the surface temperature T_b of the base tube and the freestream temperature T_∞. The circumferential temperature variations were quite small, as evidenced by the fact that the largest measured deviation of $(T_b - T_\infty)$ from $\overline{(T_b - T_\infty)}$ was about 4%.

In accordance with finned tube practice, the heat transfer surface area has been expressed as $(A_b + \eta A_f)$, where A_b is the exposed area of the base tube and A_f is the area of the fins, including both the annular faces and the tips. The fin efficiency η which multiplies A_f is an unknown and was found here by an iterative procedure in conjunction with the results of ref. [10]. In [10], the conventional one-dimensional model was used to determine the dependence of η on the fin dimensions, the fin thermal conductivity, and the heat transfer coefficient (which, in the model, is assumed uniform).

To begin the iteration, η was taken to be 1 and h was evaluated from equation (4) using the experimental data. With this h, a value of η was read from Table 2-2 of [10], which enabled equation (4) to be re-evaluated to yield a new h. In turn, a new η was obtained from [10], and the procedure was continued to convergence, yielding final values for both η and h.

It may be noted that in practice the heat transfer coefficient is not uniform along the fin surface, so that the η values obtained from the conventional fin model are of uncertain accuracy. Fortunately, such uncertainties are not reflected in the accuracy of the heat transfer coefficients evaluated from equation (4), since, by design, the efficiencies of the present fins were near unity.

In dimensionless form, the heat transfer coefficients from equation (4) were represented by the Nusselt number

$$Nu = hD/k \tag{5}$$

in which D is the diameter of the base tube and k is the thermal conductivity of air evaluated at the film temperature $\frac{1}{2}(\overline{T}_b + T_\infty)$. Since air was the heat transfer medium, the Prandtl number was virtually constant and equal to approx. 0.7.

The array pressure drop Δp, measured between static taps situated well upstream and well downstream of the array (as described earlier), was made dimensionless by means of the velocity head $\frac{1}{2}\rho U^2$. The ratio $\Delta p/\frac{1}{2}\rho U^2$ is often referred to as the pressure loss coefficient and may be represented by the symbol K_p. In reality, two different velocity heads were used in order to achieve alternative representations of the results.

One, based on the freestream velocity U_∞ upstream of the array, is

$$K_{p\infty} = \Delta p/\tfrac{1}{2}\rho U_\infty^2. \tag{6}$$

The other is based on the superficial velocity in the minimum free flow area between tubes, which includes both the spaces between the fins of each tube and the space between the fin tips of adjacent tubes. This velocity is, nominally, the maximum velocity in the array and will be denoted by U_m. If the density difference between the freestream and the minimum area is neglected, then

$$U_m/U_\infty = (s+t)S_T/[(s+t)\Delta + s(D_f - D)] \tag{7}$$

and

$$K_{pm} = \Delta p/\tfrac{1}{2}\rho U_m^2. \tag{8}$$

The density appearing in equations (7) and (8) was evaluated at the static pressure upstream of the array and at T_∞. Note that the pressure drop data were collected under isothermal conditions, so that T_∞ prevailed throughout the entire measurement zone.

Two Reynolds numbers were also used in the characterization of the heat transfer and pressure drop results, namely, Re_∞ and Re_m, with the respective definitions

$$Re_\infty = \rho U_\infty D/\mu, \quad Re_m = \rho U_m D/\mu \tag{9}$$

where D is the diameter of the base tube. The properties ρ and μ were evaluated at $\frac{1}{2}(\overline{T}_b + T_\infty)$ and at T_∞.

respectively for the heat transfer and pressure drop runs, and at the upstream static pressure (for ρ).

HEAT TRANSFER RESULTS

One-row arrays

The Nusselt number results for the one-row array are presented in Figs. 3 and 4. In the first of these, Nu is plotted as a function of the freestream Reynolds number Re_∞, while the second presents Nu as a function of the minimum-area Reynolds number Re_m. In both figures, the data are parameterized by the dimensionless transverse pitch S_T/D_f over the range from 1.07 to 3.56.

With regard to Fig. 3, a fixed value of Re_∞ corresponds to a fixed mass flowrate approaching the array and passing through it. Furthermore, the Nusselt number is a direct reflection of the heat transfer coefficient since the characteristic dimension D was fixed throughout the experiments. Therefore, the figure shows how the heat transfer coefficient for the one-row array responds to changes in the transverse pitch at a fixed mass flow. As expected, the transfer coefficient increases monotonically as the pitch decreases. The extent of the increase is appreciable; for example, in the S_T/D_f range between 1.52 and 1.07, Nu increases by about 35%. The heat transfer enhancement is accompanied by a pressure drop penalty, as will be exhibited later.

At a given transverse pitch, the Nusselt number increases monotonically with the freestream Reynolds number. The increase is logarithmically linear at the larger pitches but tends to become curved at the lower pitches. The data for each given pitch have been interconnected with a smooth curve for continuity.

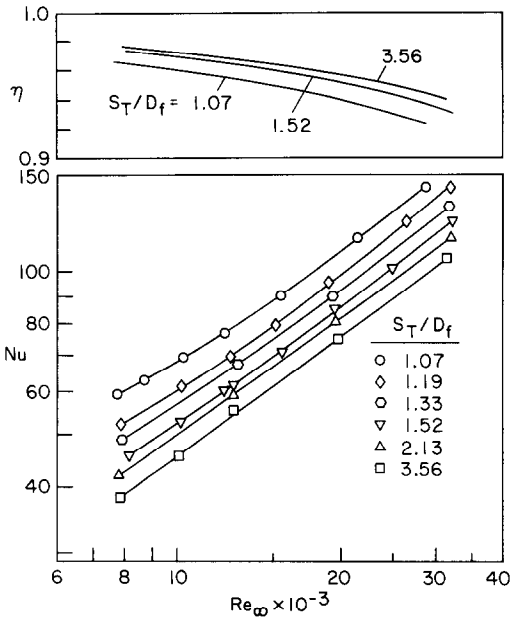

FIG. 3. Nusselt numbers and fin efficiencies for the one-row arrays plotted vs the freestream Reynolds number.

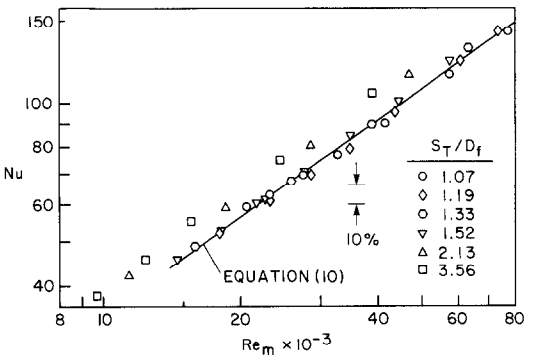

FIG. 4. Nusselt numbers for the one-row arrays plotted vs the minimum-area Reynolds number.

A major cause of the aforementioned pitch-related increase in the Nusselt number is the high velocities in the interfin and intertip spaces which accompany a reduction of the pitch at a fixed freestream velocity. This suggests the possibility of correlating the Nusselt number results by using the minimum-area Reynolds number Re_m as the independent variable, and Fig. 4 has been prepared in this regard. Inspection of the figure shows that for $S_T/D_f \leqslant 1.52$, there is a very good correlation between Nu and Re_m, independent of S_T/D_f. This is the range of S_T/D_f that is most relevant to practice. The data in this range have been fit with a least-squares power law having the equation

$$Nu = 0.0529\, Re_m^{0.704}. \tag{10}$$

This equation is plotted in Fig. 4. Of the 26 data points used to develop the correlation, 19 fall within $\pm 3\%$ of the correlating line.

The data for the two largest S_T/D_f, 2.13 and 3.56, fall 10–15% above the correlating line. These cases correspond to arrays that are much more open than the others, and it is not surprising that they do not adhere to a correlation which is appropriate to more tightly packed arrays. Another factor possibly contributing to the separateness of the results for the larger S_T/D_f is that the corresponding arrays contained relatively few tubes and may, therefore, have provided a lesser approximation to an infinitely wide array.

Attention is now turned to the fin efficiencies for the one-row array, and representative results, plotted as η vs Re_∞, are presented in the inset of Fig. 3. These results correspond to the smallest investigated S_T/D_f (= 1.07), to an intermediate S_T/D_f (= 1.52), and to a large S_T/D_f (= 3.56). The η values displayed in the figure are generally high, with an overall range from 0.92 to 0.98. These small deviations from unity reflect the use of fins having high thermal conductivity (aluminum) and moderately large thickness (0.106 cm).

As also seen in the figure, η decreases both with increasing Re_∞ and decreasing S_T/D_f, both of which tend to increase the heat transfer coefficient. Thus, the

results confirm the expectation that η decreases as the heat transfer coefficient increases for fins of fixed dimensions and thermal conductivity.

Representative results for the circumferential distribution of the base tube temperature are presented in Fig. 5. The ordinate is the ratio of the local tube-to-freestream temperature difference $(T_b - T_\infty)$ to the circumferential-average temperature difference $\overline{(T_b - T_\infty)}$. This ratio is plotted as a function of the coordinate β which specifies the angular position around the circumference of the base tube. The forward stagnation point corresponds to $\beta = 0°$, while the rear stagnation point is at $\beta = 180°$. Owing to symmetry, only the range between $\beta = 0°$ and 180° need be considered. The figure includes results for the entire investigated range of transverse spacings (S_T/D_f between 1.07 and 3.56) and corresponds to minimum-area Reynolds numbers Re_m in the neighborhood of 27,000.

It is seen from the figure that the base tube temperature takes on its lowest value at the forward stagnation point and increases monotonically with β, attaining a maximum at the rear stagnation point. The extent of the circumferential variation of the base tube temperature is small, consistent with the high conductivity and thick wall of the tube. The maximum deviation of $(T_b - T_\infty)$ from $\overline{(T_b - T_\infty)}$ is about 4%. Further inspection of the figure shows that $(T_b - T_\infty)/\overline{(T_b - T_\infty)}$ is little affected by S_T/D_f.

The circumferential distribution of $(T_b - T_\infty)$ provides a qualitative indication of the circumferential distribution of the local heat transfer coefficient, with lower values of $(T_b - T_\infty)$ corresponding to higher coefficient values and vice versa. Thus, the highest heat transfer coefficient occurs at the forward stagnation point and the lowest coefficient at the rear stagnation point. Note that because of circumferential heat conduction, the local heat flux is unknown, so that the local heat transfer coefficient does not follow directly from $(T_b - T_\infty)$.

Two-row, in-line arrays

As noted earlier, the experiments for the two-row arrays were performed for a fixed, practically-relevant transverse pitch ($S_T/D_f = 1.52$) and for six parametric values of the longitudinal pitch. As a consequence of the fixed transverse pitch, U_m/U_∞ was also fixed and equal to 1.78, so that

$$Re_m = 1.78\, Re_\infty. \tag{11}$$

In view of this, logarithmic graphs of Nu vs Re_∞ and of Nu vs Re_m convey identical information, and only one of the two formats need be presented. Here, the Nu vs Re_∞ format will be used.

The Nusselt numbers for the first and second rows of the investigated two-row, in-line arrays are presented in Figs. 6 and 7, and the discussion of results will begin with the first of these figures. As seen there, the data for the first row of the two-row array are supplemented by a line (taken from Fig. 3) which represents the Nusselt numbers for a one-row array.

An overview of Fig. 6 shows that the first-row Nusselt numbers are quite insensitive to the longitudinal pitch and do not differ significantly from those for the one-row array, which serve as a lower bound. At the lowest Reynolds number, all of the data fall together, regardless of the longitudinal pitch. The sensitivity of the data to the pitch increases with increasing Reynolds number, but even at the largest Reynolds number, the pitch-related spread of the data is only about 10%.

The Nusselt numbers corresponding to the largest investigated pitch, $S_L/D_f = 5.20$, are coincident with those for the one-row array at all Reynolds numbers, while the Nusselt numbers for the $S_L/D_f = 3.10$ pitch deviate by no more than 2%. Therefore, as far as the first-row heat transfer is concerned, the two-row array behaves like a one-row array for $S_L/D_f > \sim 3$.

For $S_L/D_f < 3$, the interactions between the rows enhance the first-row heat transfer, albeit moderately. In this regard, it is reasonable to expect that the presence of the second row would affect the nature of

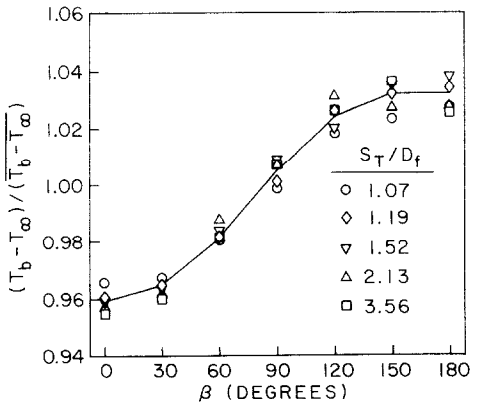

FIG. 5. Circumferential distributions of the base tube temperature.

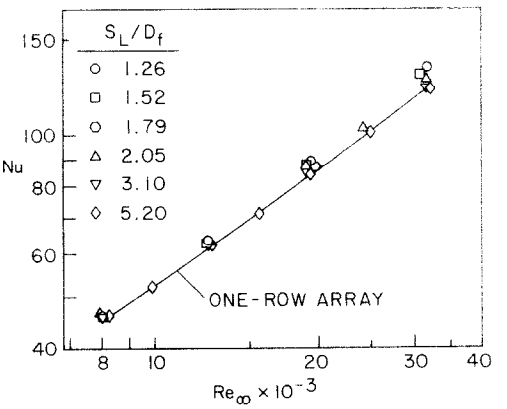

FIG. 6. Nusselt numbers for the first row of the two-row, in-line arrays.

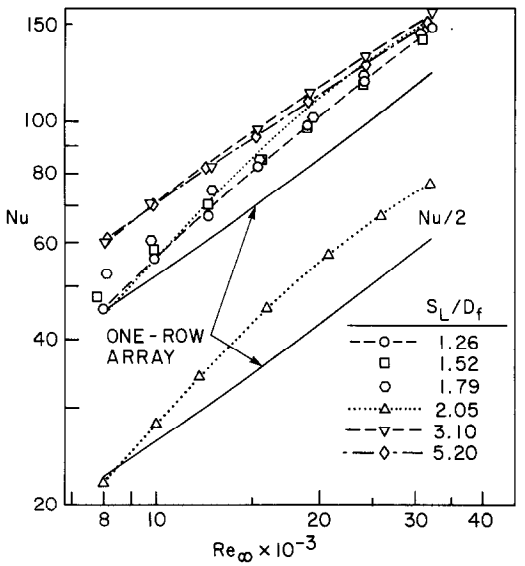

FIG. 7. Nusselt numbers for the second row of the two-row, in-line arrays.

the wake shed by the first row and, by this means, alter the heat transfer. However, heretofore, it was not known whether the first-row heat transfer would be increased or decreased by the presence of the second row. The fact that the actual effect is so small is, in itself, somewhat surprising.

Attention is next turned to Fig. 7 and to the heat transfer results for the second row of the two-row, in-line arrays. In the upper part of the figure, the Nu, Re_∞ data corresponding to each of the six indicated longitudinal pitches are plotted along with a reference line which represents the data for the one-row array. As designated in the legend, faired curves were used to interconnect certain of the data, but other data were left without interconnecting lines to avoid excessive entanglement. Also, to preserve clarity, the data for the $S_L/D_f = 2.05$ pitch, which tend to cut across the data for the other pitches, are not shown as such in the upper part of the figure. Rather, these data have been plotted as $\frac{1}{2}Nu$ and appear in the lower part of the figure along with the one-row-array reference line.

From an overall inspection of Fig. 7, taking account of Fig. 6 and of the reference line which is common to both figures, it is seen that the Nusselt numbers for the second row of the array exceed those for the first row. This trend is common to all tube-bundle-type heat exchangers and is due to the turbulence spawned by the first row which impinges on the second row. The maximum increase of the second-row Nusselt numbers relative to those of the first row is about 35%. Increases of this general magnitude occur at the two largest longitudinal pitches ($S_L/D_f = 3.10$ and 5.20) over the entire investigated range of Reynolds numbers. However, lesser increases may occur at smaller longitudinal pitches, especially at lower Reynolds numbers. Indeed, at low Reynolds numbers and $S_L/D_f < \sim 1.5$, the second-row Nusselt numbers are only slightly larger, if at all, than the first-row Nusselt numbers.

Further examination of Fig. 7 reveals that the dependence of the second-row Nusselt number on the longitudinal pitch is substantially affected by the magnitude of the Reynolds number. At the lower end of the Reynolds number range, the Nusselt number at first increases monotonically with increasing longitudinal pitch up to $S_L/D_f = 1.79$ but unexpectedly decreases at $S_L/D_f = 2.05$ and then increases again as S_L/D_f further increases. On the other hand, in the high Reynolds number range, the Nusselt number is relatively insensitive to longitudinal pitch and, for all pitches, substantially exceeds the one-row value. The maximum Nusselt number appears to occur at the next-to-largest longitudinal pitch, suggesting that the inevitable decay of the turbulence with increasing longitudinal distance between the rows is already taking place at the largest pitch.

The complex behavior described in the preceding paragraphs is believed to be related to whether the second row is immersed in the wake of the first row or is situated downstream of the closure of the wake. For example, moderate fluctuations of the measured base tube temperatures were recorded at the lower Reynolds numbers for $S_L/D_f = 2.05$ (and only for these cases). This is interpreted as suggesting that for these cases, the wake closure occurred immediately upstream of the second row, and the waving tail of the wake destabilized the flow washing over the second-row tubes.

Because of space limitations, results for the fin efficiency and for the circumferential distribution of the base tube temperature will not be presented here for the two-row, in-line arrays. This information is available in ref. [9].

Two-row, staggered arrays

The experiments for the two-row, staggered arrays were carried out for the same fixed transverse pitch ($S_T/D_f = 1.52$) and for the same parametric values of the longitudinal pitch as for the in-line arrays. The Nusselt number results for the first and second rows of the staggered arrays are respectively presented in Figs. 8 and 9.

In the upper part of Fig. 8, the first-row Nu vs Re_∞ data for all the investigated longitudinal pitches are plotted along with a solid line which represents the one-row Nusselt number results from Fig. 3. A replot of the data for the $S_L/D_f = 1.79$ pitch as $\frac{1}{2}Nu$ appears in the lower part of the figure, as does the one-row line which serves as a reference.

From the figure, it is seen that the first-row Nusselt numbers are bounded from below by those for the one-row array. Furthermore, both in the practical range of moderate longitudinal pitches $S_L/D_f = 1.26$–1.52 and in the large-pitch range, $S_L/D_f = 3.10$–5.20, the Nusselt numbers are quite insensitive to pitch and deviate only slightly (by no more than about 4%) from the line representing the one-row results. However, between

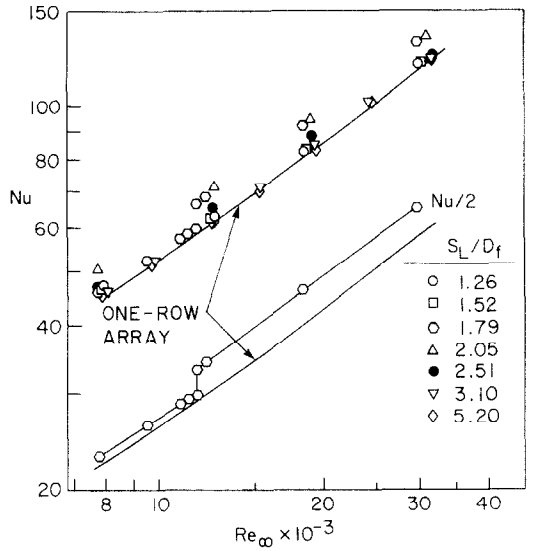

FIG. 8. Nusselt numbers for the first row of the two-row, staggered arrays.

these ranges, the data unexpectedly display both greater sensitivity to pitch and greater deviations from the line.

The Nu, Re_∞ distribution for the $S_L/D_f = 1.79$ pitch suggests the existence of a transition in the pattern of fluid flow in the neighborhood of $Re_\infty = 11{,}800$, and this conjecture is supported by observed fluctuations in the measured base tube temperatures at that Reynolds number. For this pitch and at Reynolds numbers below the transition, the Nusselt numbers exceed the one-row values by about 4%, while above the transition the deviations are about 15%. The post-transition flow pattern appears to persist for the next larger longitudinal pitch, $S_L/D_f = 2.05$, since the Nusselt numbers remain high (12–15% above the one-row line). On the other hand, the Nusselt numbers for the next longitudinal pitch, $S_L/D_f = 2.51$ (an additional case introduced to obtain more detail), show a decline relative to the aforementioned high values.

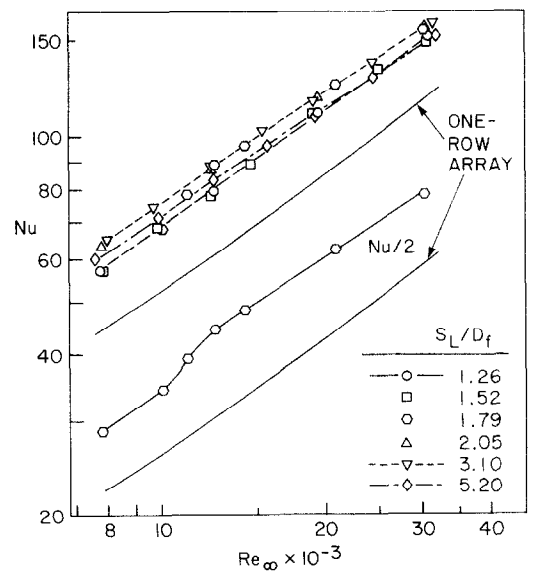

FIG. 9. Nusselt numbers for the second row of the two-row, staggered arrays.

The behavior described in the preceding paragraphs deviates from expectations. In the staggered arrangement, the presence of the second row would be expected to constrain the width of the wakes spawned by the first-row tubes, especially at the smaller longitudinal pitches. Correspondingly, the most marked effects of the presence of the second row should occur at these pitches. The fact that the largest effects actually occurred at intermediate pitches suggests complexities in the flow field beyond those that are intuitively apparent.

The first-row Nusselt numbers for the staggered and in-line arrays may be compared by reference to Figs. 8 and 6. For the $S_L/D_f = 2.05$ pitch and for $Re_\infty > 11{,}800$ for the $S_L/D_f = 1.79$ pitch, the staggered array clearly yields higher Nusselt numbers. However, for the practically-relevant range of smaller S_L/D_f, the comparison is not clearly conclusive unless it is made on a Reynolds-number-by-Reynolds-number basis and, in any event, the differences are generally small.

The Nusselt numbers for the second row of the investigated two-row, staggered arrays are presented in Fig. 9 in a now-familiar format. These Nusselt numbers are seen to fall in a band that is 30–45% above the line for the one-row array. Thus, the second-row heat transfer is definitely enhanced relative to the first-row heat transfer for all operating conditions.

Overall, the Nusselt number at first increases with increasing longitudinal pitch, attains a maximum, and then decreases with further increases in pitch. The increase occurs for pitches greater than $S_L/D_f \sim 1.5$, and the maximum is attained at $S_L/D_f = 2.05$ and 3.10 over the entire Reynolds number range and at $S_L/D_f = 1.79$ for $Re_\infty > 12{,}000$. The Nu, Re_∞ distribution for the latter S_L/D_f displays a localized rapid rise which is related to the flow pattern transition already discussed in connection with the first-row Nusselt number results.

In the staggered arrangement, the second row is positioned in the jet-like streams which emerge from the intertube spaces of the first row. The higher velocity and higher turbulence of these streams (relative to those of the freestream) are responsible for the significant enhancement in evidence in Fig. 9. The turbulence intensity is believed to increase with increasing S_L, attain a maximum, and then decrease, while the jet-stream velocity decreases as the velocity field becomes more homogeneous with S_L. Thus, the pitch-related maximum in the Nusselt number is due to the action of the turbulence intensity.

A comparison of the second-row Nusselt number for the staggered and in-line arrays (Figs. 9 and 7) shows that the former are generally higher. For example, the maximum enhancement (relative to the one-row results) is 45% for the staggered arrays and 35% for the

in-line arrays. Furthermore, the enhancement is more uniform with respect to S_L for the staggered array. Careful inspection of Figs. 7 and 9 shows that the Nusselt numbers for the largest investigated longitudinal pitch ($S_L/D_f = 5.20$) are virtually the same for the two types of arrays.

The fin efficiencies and base tube temperature distributions for the two-row, staggered arrays are available in ref. [9].

FLUID FLOW RESULTS

Upstream velocity field

As described in the Apparatus section, supplementary data runs were made with an L-shaped impact probe installed immediately upstream of the array to explore possible disturbances of the approach flow caused by the blockage created by the array. The tip of the probe was situated about 2.5 cm upstream of the forward edge of the array (this was as close as the tip could be positioned with respect to the array). Traverses in the spanwise direction sensed the flow upstream of both the tubes and the intertube spaces. From such traverses performed for all the arrays, the velocity was found to be uniform and equal to that in the approach flow well upstream of the array.

These results show that for the investigated Reynolds number range, the presence of the array was not felt very far upstream. Rather, the turning of the flow to accommodate the blockage was accomplished very close to the forward edge of the array.

Traverses were also made in the direction of the tube axes (i.e. in the vertical direction). These traverses affirmed that the test portion of the heated tube was well outside the wall boundary layers of the wind tunnel.

Pressure drop for one-row arrays

The measured overall pressure drops for the one-row arrays are presented in dimensionless terms by means of the pressure loss coefficients $K_{p\infty}$ and K_{pm} defined by equations (6) and (8). These results are respectively plotted in Figs. 10 and 11 for parametric values of the dimensionless transverse pitch S_T/D_f. In both figures, the data for each pitch have been interconnected by a smooth curve for continuity.

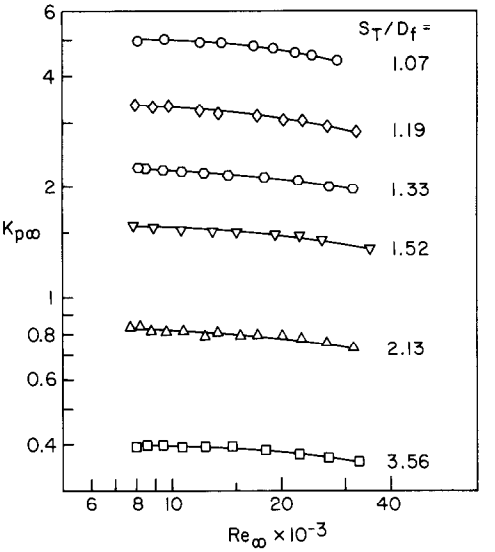

FIG. 10. Pressure loss coefficients for the one-row arrays plotted vs the freestream Reynolds number.

Since U_∞ appears in both the ordinate and the abscissa variables of Fig. 10, the figure can be interpreted as showing how the array pressure drop responds to changes in the transverse pitch for a fixed freestream velocity. As expected, the pressure drop increases markedly with decreasing pitch (i.e. increasing blockage), the increase being, for example, about a factor of three in the range between $S_T/D_f = 1.52$ and 1.07. These are the pressure drop penalties that are paid for the pitch-related increases in the Nusselt number that were exhibited in Fig. 3.

It is also seen from Fig. 10 that $K_{p\infty}$ is not quite constant with Re_∞, as would be true if the pressure drop were due solely to inertial losses. The slight decrease of $K_{p\infty}$ with Re_∞ reflects the fact that the increase of the

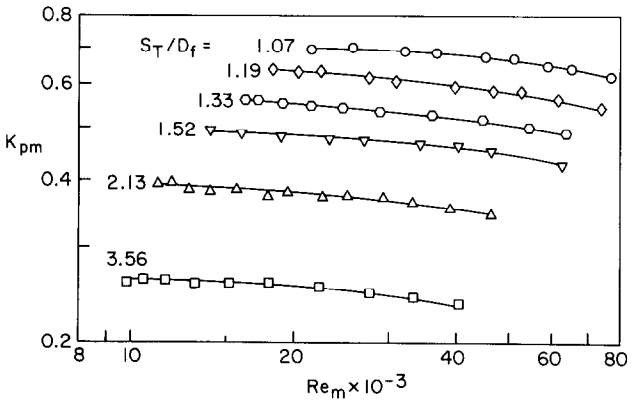

FIG. 11. Pressure loss coefficients for the one-row arrays plotted vs the minimum-area Reynolds number.

friction-related pressure drop with velocity is less rapid than U_∞^2.

The rephrasing of the pressure drop results in terms of the minimum-area velocity U_m reduces the overall spread in the pressure loss coefficient to a factor of three (compared with a factor of 12 for $K_{p\infty}$), as can be seen in Fig. 11. The fact that the use of U_m does not bring the data into complete congruence can be explained by noting that the minimum free flow area based strictly on the geometry of the system is not the actual minimum free flow area. The deviation is due to the vena contracta effect.

To illustrate this point, consider the $S_T/D_f = 1.07$ pitch, the smallest pitch. For this case, the change in cross section from the freestream to the minimum free flow area corresponds very nearly to an infinite contraction ratio, so that the contraction coefficient can be taken as 0.6. If U_m were to be redefined using this contraction coefficient, the resulting pressure loss coefficient would be about 0.25. On the other hand, for the $S_T/D_f = 3.56$ pitch, the largest pitch, the contraction is so slight that the vena contracta effect is negligible, and the K_{pm} values of Fig. 11, which are about 0.25, are appropriate. Thus, a proper accounting of the actual minimum free flow area brings all the dimensionless pressure drop data together.

Pressure drop for two-row arrays

The pressure loss coefficients representing the overall pressure drop data for the two-row staggered and in-line arrays are respectively presented in Figs. 12(a) and (b) for parametric variations of the dimensionless longitudinal pitch S_L/D_f. As noted earlier in connection with the Nusselt number presentation, the fixed transverse pitch ($S_T/D_f = 1.52$) means that no new information is provided by using U_m as an alternative to U_∞ for the reference velocity. Therefore, Fig. 12 is based on U_∞ (i.e. $K_{p\infty}$ plotted vs Re_∞). For reference purposes, the one-row $K_{p\infty}$ data corresponding to $S_T/D_f = 1.52$ are plotted in both the (a) and (b) parts, as are the doubled one-row $K_{p\infty}$ data.

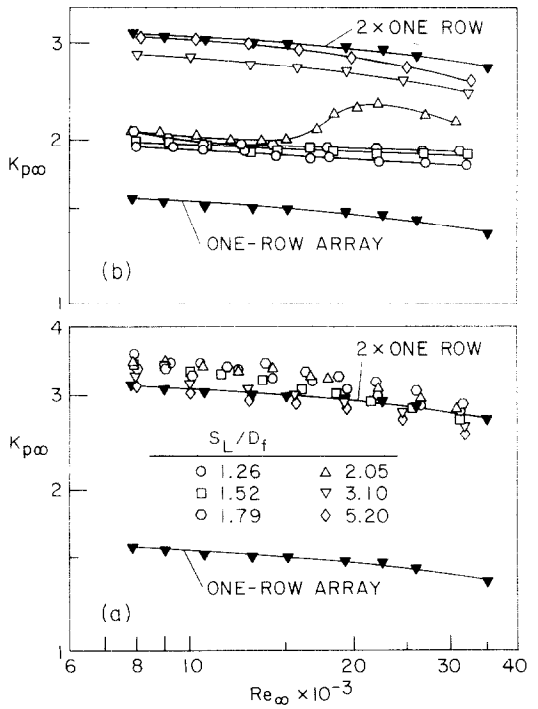

FIG. 12. Pressure loss coefficients for the two-row arrays; (a) staggered, (b) in-line.

A comparison of the two parts of the figure reveals marked differences between the pressure drop results for the staggered and in-line arrays. For the staggered arrays, $K_{p\infty}$ is remarkably insensitive to the longitudinal pitch, with the spread in the data at a fixed Reynolds number being about 15% over the entire range of S_L/D_f from 1.26 to 5.20. Furthermore, the $K_{p\infty}$ values do not differ appreciably from double those of the one-row array.

The $K_{p\infty}$ values for the in-line arrays are generally smaller than those for the staggered arrays, which is consistent with literature information for unfinned tube bundles. In the practically-relevant range of moderate longitudinal pitches, i.e. $S_L/D_f \leqslant 1.79$, the in-line $K_{p\infty}$ values depend only slightly on S_L/D_f and are 55–65% of those for the staggered array. The in-line $K_{p\infty}$ data for the $S_L/D_f = 2.05$ pitch reflect a transitional fluid flow pattern which, as discussed in connection with the Nusselt number results of Fig. 7, is attributed to the changeover from immersion of the second row in the first row's wake to closure of the wake in front of the second row. Evidently, the latter flow pattern gives rise to higher pressure drops, as is evidenced by the relatively high $K_{p\infty}$ values for $S_L/D_f = 2.05$ at larger Re_∞ and for $S_L/D_f = 3.10$, which, however, are still below those for the staggered array. Only at the largest longitudinal pitch, $S_L/D_f = 5.20$, are the results for the two types of arrays virtually coincident.

In light of the foregoing, it is seen that the higher Nusselt numbers for the staggered arrays, relative to those for the in-line arrays, are achieved at the price of substantial pressure drop penalties, especially for $S_L/D_f \leqslant 1.79$.

COMPARISONS WITH LITERATURE INFORMATION

As noted in the Introduction, no information was found in the published literature for one- or two-row finned tube arrays. Therefore, only limited comparisons can be made between the present results and the literature.

Heat transfer

The only heat transfer comparison that appears possible is that between the first row of the present two-row, staggered arrays and the first row of the eight-row, staggered arrays investigated in ref. [3]. According to [3], the eight-row Nusselt number correlation given

there should be derated by 29% for the first row, but the presentation is so concise that the data on which the derating factor is based are not documented. The experiments of [3] were performed with helically-finned tubes (in contrast to the present annular-finned tubes), for a limited range of S_L/D_f, and for values of S_T/D_f that were, for the most part, larger than the 1.52 of the present two-row arrays. Furthermore, a two-fluid heat exchanger was used in [3], while the present experiments were performed with a one-fluid, electrically-heated apparatus.

The comparison of Nusselt number results for the range of S_L/D_f common to the two sets of data is shown in Fig. 13(a). Despite the differences cited in the preceding paragraph, there is generally good agreement between the present data and the lines which represent the correlation of [3]. This agreement both reinforces the quality of the data and the utility of the correlating equation.

Pressure drop

Per-row pressure drop correlations for staggered, many-rowed arrays are presented in refs. [1] and [3], based on experiments with helically-finned tubes. These correlating equations have been utilized to provide comparisons with the present $K_{p\infty}$ data for two-row, staggered arrays, and the comparisons are shown in Fig. 13(b). Note that each correlation has been employed only for the range of S_L/D_f for which it is applicable.

Inspection of the figure shows that the data fall within the band defined by the correlating lines. The lines are seen to be more sloped than the data, suggesting that friction-related pressure losses play a greater role in helically-finned arrays than in annular-finned arrays. It may also be observed that there are substantial differences (up to 35%) between the correlations set forth in [1] and [3].

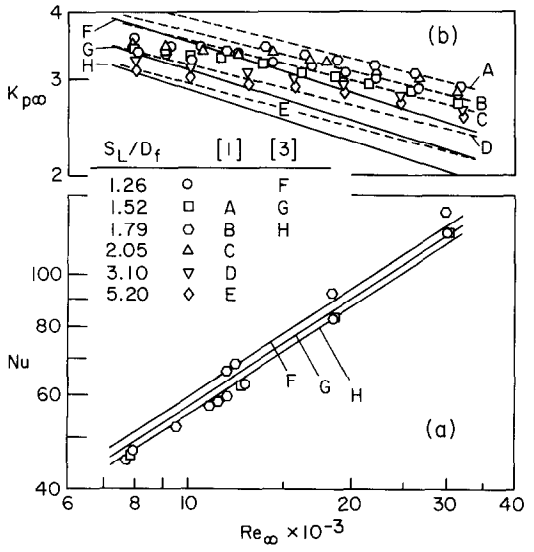

FIG. 13. Comparisons with literature information; (a) Nusselt numbers, (b) pressure loss coefficients.

CONCLUDING REMARKS

The heat transfer and pressure drop characteristics of one- and two-row arrays of annular-finned tubes have been determined from airflow experiments. For the one-row arrays, the transverse pitch was varied parametrically. The two-row arrays were investigated for both the in-line and staggered configurations at a fixed, practically-relevant transverse pitch and for parametric values of the longitudinal pitch. For each of the investigated geometries, the Reynolds number, based on the freestream velocity and on the diameter of the base tube, was varied from 7500 to 32,000.

The Nusselt numbers for the one-row arrays increased with decreasing transverse pitch. For example, in the practically-relevant range of S_T/D_f between 1.52 and 1.07, the increase in the Nusselt number was about 35%, while the pressure drop increased by a factor of three. In this range, the heat transfer data were well correlated by the equation, $Nu = 0.0529\, Re_m^{0.704}$, independent of the transverse pitch, where Re_m is based on the velocity in the geometrical minimum free flow area. It was also found that the pressure drop data could be brought together provided that the pressure loss coefficient was based on the velocity at the actual minimum free flow area.

For the first row of the two-row, in-line arrays, the Nusselt numbers were quite insensitive to the longitudinal pitch and did not differ significantly from those for the one-row array. The Nusselt numbers for the second row generally exceeded those for the first row (up to 35%), but the extent of the increase was sensitive to both the longitudinal pitch and the Reynolds number. At smaller longitudinal pitches ($S_L/D_f \leqslant 1.52$) and lower Reynolds numbers ($Re_\infty \sim 8000$), the increase was less than 10%, if at all. The pressure drops for the two-row, in-line arrays were generally less than twice those of the corresponding one-row array, with an overall trend for the pressure drop to increase with increasing longitudinal pitch.

The first-row Nusselt numbers for the two-row, staggered arrays differed only slightly from those for the one-row array, both for the practical range of moderate longitudinal pitches and in the large-pitch range. Between these ranges, the Nusselt number displayed both greater sensitivity to pitch and greater deviations from the one-row values. The second-row Nusselt numbers for all the investigated longitudinal pitches fell in a band that was 30–45% above those for the one-row array. Similarly, the pressure drops for the two-row, staggered arrays were found to be insensitive to the pitch, with values that were about twice those of the one-row array.

Overall, an in-line array yielded lower Nusselt numbers than did the corresponding staggered array, but with a lower pressure drop. For example, in the range of moderate longitudinal pitches (i.e. $S_L/$

$D_f \leqslant 1.79$), the in-line-array pressure drops were 55–65% of the staggered-array pressure drops.

Representative results were also presented for the fin efficiency and for the circumferential variation of the base tube temperature.

REFERENCES

1. S. L. Jameson, Tube spacing in finned-tube banks, *Trans. Am. Soc. mech. Engrs* **67,** 633–642 (1945).
2. C. Rounthwaite and N. Cherrett, Heat transfer and pressure drop performance of helically finned tubes in staggered crossflow, *J. Br. Nucl. Energy Conf.* **6,** 300–306 (1961).
3. Z. Mirkovic, Heat transfer and flow resistance correlation for helically finned and staggered tube banks in crossflow. In *Heat Exchangers: Design and Theory Sourcebook* (Edited by N. Afgan and E. U. Schlunder). Scripta, Washington (1974).
4. J. W. Ackerman and A. R. Brunsvold, Heat transfer and draft loss performance of extended surface tube banks, *J. Heat Transfer* **92,** 215–220 (1970).
5. A. Lymer, Finned tubes and their performance characteristics, *Nucl. Engng* **2,** 504–509 (1957).
6. S. B. H. C. Neal and J. A. Hitchcock, A study of the heat transfer processes in banks of finned tubes in crossflow, using a large scale model technique, *Proc. 3rd Int. Heat Transfer Conference*, Vol. 3, pp. 290–298, Chicago (1966).
7. J. C. Biery, Prediction of heat transfer coefficients in gas flow normal to finned and smooth tube banks, *J. Heat Transfer* **103,** 705–714 (1981).
8. A. Y. Gunter and W. A. Shaw, A general correlation of friction factors for various types of surfaces in crossflow, *Trans. Am. Soc. mech. Engrs* **67,** 643–660 (1945).
9. F. Samie, Effect of inclination, transverse intertip spacing, and longitudinal pitch on crossflow heat transfer from an array of finned tubes. Ph.D. thesis, Department of Mechanical Engineering, University of Minnesota, Minneapolis, Minnesota (1984).
10. D. Q. Kern and A. D. Kraus, *Extended Surface Heat Transfer*. McGraw-Hill, New York (1972).

TRANSFERT THERMIQUE ET PERTE DE CHARGE POUR DES TUBES AILETES DISPOSES EN UNE OU DEUX NAPPES

Résumé—Des expériences sont conduites pour déterminer les nombres de Nusselt et les coefficients de perte de charge pour des tubes à ailettes annulaires disposés en une seule nappe ou en deux nappes en ligne ou en quinconce. L'appareil est chauffé électriquement et l'air est le fluide de travail. Les pas transverses et longitudinaux sont variables et, pour chaque configuration, le nombre de Reynolds d'écoulement libre varie de 7500 à 32 000. Pour les arrangements à une nappe, le nombre de Nusselt et le coefficient de perte de charge sont très sensibles au pas transverse. Les nombres de Nusselt pour la première nappe ou pour les deux nappes ne sont pas nettement différents de ceux de la nappe unique correspondante, avec la plus grande déviation apparaissant pour des nappes en quinconce ayant des valeurs intermédiaires du pas longitudinal. Pour les tubes de la seconde nappe, les nombres de Nusselt des nappes en quinconce dépassent généralement ceux des nappes en ligne et sont aussi moins sensibles au pas longitudinal. Les pertes de charge globales pour les deux nappes, avec quinconce, sont aussi presque insensibles au pas, avec des valeurs qui sont deux fois ceux de l'arrangement correspondant à une seule nappe. D'autre part, les pertes de charge pour les arrangements en ligne sont toujours moindre que deux fois les valeurs pour une seule nappe, avec une tendance à l'accroissement quand on augmente le pas longitudinal.

ERGEBNISSE FÜR DEN WÄRMEÜBERGANG UND DRUCKABFALL FÜR EIN- UND ZWEIREIHIGE RIPPENROHR-ANORDNUNGEN

Zusammenfassung—Es wurden Messungen durchgeführt, um die Nußeltzahlen und die Druckabfallkoeffizienten für Rohre mit Kreisrippen zu bestimmen, wobei die Rohre entweder in einer Reihe angeordnet waren, oder zweireihig fluchtend oder versetzt. Der Apparat wurde elektrisch beheizt, und die Wärmeübertragung erfolgte konvektiv an Luft. Die Längs- und Querteilung wurde systematisch verändert, wobei für jede Konfiguration der Bereich der Reynoldszahl der ungestörten Strömung zwischen 7500 und 32000 lag. Bei den Anordnungen in einer Reihe waren die Nußelt-Zahl und der Druckabfallkoeffizient in hohem Maße von der Querteilung abhängig. Die Nußelt-Zahlen an der ersten von zwei Reihen unterschieden sich nur unmerklich von denen für die entsprechende einreihige Anordnung, wobei die größten Abweichungen bei der versetzten Anordnung mit mittleren Werten der Längsteilung auftraten. Für die Rohre der zweiten Reihe waren die Nußelt-Zahlen bei der versetzten Anordnung stets erheblich größer als bei fluchtender Anordnung; die Längsteilung spielte keine große Rolle. Der Gesamtdruckabfall bei zweireihiger, versetzter Anordnung hing ebenfalls wenig von der Teilung ab, wobei die Werte etwa doppelt so groß wie bei der entsprechenden einreihigen Anordnung waren. Andererseits waren die Druckabfallwerte bei fluchtender Anordnung weniger als zweimal so groß wie bei einer Reihe. Es bestand eine Tendenz zu größeren Werten mit zunehmender Längsteilung.

РЕЗУЛЬТАТЫ ПО ТЕПЛООБМЕНУ И ПЕРЕПАДУ ДАВЛЕНИЯ ДЛЯ ОДНО-И ДВУХРЯДНЫХ ПУЧКОВ ИЗ ОРЕБРЕННЫХ ТРУБ

Аннотация—Проведены эксперименты по измерению чисел Нуссельта и потери давления для поперечно оребренных труб, установленных либо в форме однорядной решетки, либо в форме двухрядного пучка с коридорным либо шахматным расположением труб. Трубы нагревались электрическим током, конвективный теплосъем осуществлялся воздухом. Поперечные и продольные шаги решеток изменялись параметрически для каждой конфигурации, а число Рейнольдса свободного потока варьировалось в диапазоне 7500–32000. Для однорядных решеток как число Нуссельта, так и потери давления сильно зависели от поперечного шага. Числа Нуссельта для первого ряда двухрядного пучка не отклоняются значительно от чисел соответствующей однорядной решетки, причем наибольшее отклонение имеет место в случае шахматного пучка с касательного напряжения на стенке стремится к бесконечности. Это имеет место для положительного касательного напряжения на стенке, т.е. до достижения классического условия отрыва. Показано, что полученный результат обусловлен механизмом самоусиления.